agriculture

MDPI

Article

Design and Optimization of a Soil-Covering Device for a Corn No-Till Planter

Yuanle Geng [1], Xianliang Wang [1,*], Xiaokang Zhong [1], Xiangcai Zhang [1], Kun Chen [1], Zhongcai Wei [1], Qingxin Lu [1], Xiupei Cheng [1] and Mingtao Wei [2]

[1] School of Agricultural Engineering and Food Science, Shandong University of Technology, Zibo 255000, China
[2] Weifang Letian Agricultural Science & Technology Co., Ltd., Weifang 261102, China
* Correspondence: wxl1990@sdut.edu.cn

Abstract: Aiming to solve the problems of easy generation of clods, poor soil fluidity and poor soil-covering effect in the no-tillage seeding operation mode, this study has designed a soil-covering device with a soil-closing function for the chisel-type furrow opener of a corn no-tillage planter. Theoretical analysis and design of the soil dividing plate and the soil-covering disc were carried out, and the key parameters were determined. Then, the soil-covering device with soil-closing function and the soil movement model was constructed in Altair EDEM, and the spatial soil particle mobility was analyzed. The numerical simulation method was combined with the center plane composite response test scheme to carry out the simulation test, and the optimal working parameter combination was obtained. The operating speed was 6.35 km·h^{-1}, the inclination angle of the soil-covering disc was 60°, the opening angle of the soil-covering disc was 70°, and the inclination angle of the soil dividing plate was 40°. A comparative test of the soil-covering effect and performance was carried out, and the results showed that the designed device was better than the traditional soil-covering device in terms of the consistency of soil-covering thickness and the stability of seed position deviation. The relative errors of the soil bin experiment results and the simulation optimization results for the cover soil thickness and seed position deviation were 5.7% and 11.1%, respectively. The operation effect of the designed soil-covering device with soil-closing function meets the requirements of soil covering under no-tillage conditions and provides a basis for the research and development of soil-covering suppression technology and devices under no-tillage seeding mode.

Keywords: no-tillage; soil cover; discrete element; soil-covering thickness; seed offset

check for updates

Citation: Geng, Y.; Wang, X.; Zhong, X.; Zhang, X.; Chen, K.; Wei, Z.; Lu, Q.; Cheng, X.; Wei, M. Design and Optimization of a Soil-Covering Device for a Corn No-Till Planter. *Agriculture* **2022**, *12*, 1218. https://doi.org/10.3390/agriculture12081218

Academic Editors: Mustafa Ucgul and Chung-Liang Chang

Received: 27 June 2022
Accepted: 11 August 2022
Published: 13 August 2022

Publisher's Note: MDPI stays neutral with regard to jurisdictional claims in published maps and institutional affiliations.

Copyright: © 2022 by the authors. Licensee MDPI, Basel, Switzerland. This article is an open access article distributed under the terms and conditions of the Creative Commons Attribution (CC BY) license (https://creativecommons.org/licenses/by/4.0/).

1. Introduction

No-till seeding technology is one of the core technologies of conservation tillage, which can not only reduce wind erosion and water erosion, and improve soil fertility and drought resistance, but also have the advantages of water conservation and moisture conservation, cost-saving and efficiency improvement, and soil fertility [1,2]. However, under the continuous no-tillage mode, the surface soil is hard, and the surface is uneven [3]. During the operation of the seeder, the chisel-type furrow opener has problems such as easy generation of clods, poor soil fluidity and a poor soil-covering effect [4], which seriously affect the sowing quality. Therefore, it is of great significance to analyze the flow characteristics of no-till soil during the operation of the chisel-type furrow opener and optimize the soil-covering device of the no-till planter to improve the quality of no-till sowing and promote conservation tillage.

The law interaction between soil and tillage components is the basis for designing and selecting soil tillage components. The discrete element method (DEM) can be used to study the flow of particulate matter and the behavior of soil fragmentation and is widely considered in the research of soil-contacting components of agricultural machinery [5,6]. Scholars have conducted extensive research on the interaction process between soil and

tillage equipment based on DEM [7–11], and these studies have confirmed the superiority of discrete element simulation of the tillage process. Compared with the traditional theoretical derivation and experimental analysis, the DEM has the advantages of saving time and labor, low cost, and visualization of results; compared with the numerical simulation method (such as the finite element method), the DEM has the model fidelity high and high accuracy of simulation results. Moreover, the movement trajectory of the grains can be tracked in the discrete element to analyze the soil particles' force and movement during the tillage process.

Presently, scholars' research on soil-covering devices mainly focuses on the shape and structure design and precise soil-covering control of soil-covering devices. In terms of the shape and structure design of the soil-covering device, Zhang et al. [12] designed a dryland auger-type precise soil-covering device, which improved the operation accuracy and soil-covering effect. Zhang et al. [13] designed a crushing soil-covering device based on bionics, which improved the crushing performance. In order to solve the problems of excessive resistance and poor soil-covering effect during the straw returning process, Lin et al. [14] designed a spiral soil-covering device. Liu et al. [15] designed a new double-layer disc-type soil-covering device, which remarkably affects soil covering, improves the sowing accuracy and reduces the displacement of seeds in the process of covering soil. At the same time, some scholars optimize the parameters of the soil-covering device through simulation analysis to improve the soil-covering effect [16–18].

Regarding precise soil cover control, that is, to achieve accurate control and real-time adjustment of the amount and thickness of soil cover. Li et al. [19] designed a cover soil-suppression linkage monitoring device to adjust the amount of cover soil in real-time. Chao et al. [20] designed an automatic adjustment device for the amount of soil covered by a transplanter to realize the automatic adjustment and control of the amount of soil covered on the membrane of the transplanter. At the same time, some scholars mainly conducted research on the control of sowing depth of precision seeding technology [21–24]. In general, the existing research on the soil-covering device mainly focuses on the depth of soil-covering and active control of the sowing depth, and there are few studies on the effect of the soil-covering device and the soil flow movement state of the soil-covering process and the displacement of the seeds after touching the soil under the no-tillage seeding mode.

Therefore, to improve the soil-covering effect of the opener of the seeder when working on the surface of no-tillage sowing, a soil-covering device with a soil-closing function was designed in this paper, and the discrete element method was used to carry out a four-factor and three-level regression combination test. The simulation model determines the optimal parameter combination of the soil-closing device and uses the soil bin experiment results to verify it to provide a theoretical basis and technical support for the precision no-tillage seeder to achieve the consistency of seeding depth and the development of the soil-covering device.

2. Materials and Methods

2.1. Design of Soil-Covering Device with Soil-Closing Function

2.1.1. Overall Design

The soil-covering device with a soil-closing function is composed mainly of a trench opener, a share shaft, a seed metering device, a soil dividing plate, and soil-covering discs. The overall structure is shown in Figure 1. The soil dividing plate is mounted on both sides of the retaining plate through the fixing holes, and the connecting frame is installed on the soil retaining plate through the chute. The two earth-covering discs are fixedly installed on the connecting frame, and the discs' inclination angle and opening angle can be changed by adjusting the fixed position of the bolts in the positioning holes. The biggest difference between the device we designed and optimized and the traditional soil-covering device is the presence or absence of the soil-dividing plate.

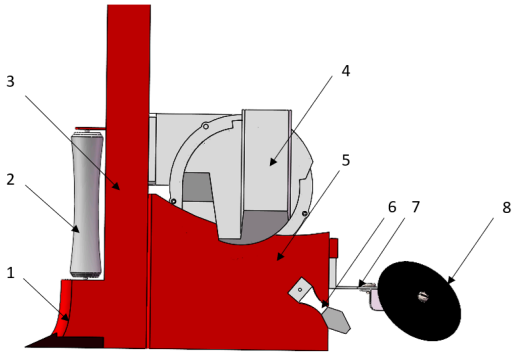


Figure 1. Schematic diagram of the overall structure of the soil-covering device with soil-closing function: 1—opener; 2—anti-blocking roller; 3—share shaft; 4—seed metering device; 5—retaining plate; 6—dividing plate; 7—connection frame; 8—covering disc.

2.1.2. Working Process

During the operation, the trench is first opened by the opener, and the front-end soil dividing plate first covers a small amount of finely divided soil on the surface of the seeds to realize the contact between the seeds and the loose and finely divided soil and complete the first covering of soil. Then, the loose soil formed by the opener after the operation is actively covered back into the seed furrow formed after ditching along the inner side of the covering disc by the soil-covering discs at the rear end to complete the second covering of the seeds. The soil covering of the device is completed in two parts. The first step is to cover a small part of the soil through the soil dividing plate to reduce the soil disturbance. The second step is to cover the soil through the discs to meet the soil-covering requirements. By adjusting the design parameters such as the opening angle, the round inclination angle and the inclination angle of the soil dividing plate, the amount of soil-covering can be adjusted, thereby changing the thickness of the soil covering of the seeds.

2.1.3. Design of Key Components

According to the soil-covering device's structure and soil dynamics model with soil-closing function, the analysis part of the soil-covering device is mainly divided into two parts: the soil dividing plate and the soil-covering discs.

When the opener is working, the soil on both sides will flow into the seed ditch by itself with the advance of the opener, which realizes the function of self-covering to a certain extent. The thickness of its self-covering soil is related to parameters such as the natural angle of repose φ of the soil particles and the distance x between the two discs. The relationship between them is shown in Figure 2. From reference [25], it is concluded that the expression of the opener after self-covering is:

$$H = H_1 - 7.245x_1^{0.367} \quad (1)$$

where H—self-covering soil thickness of the opener (mm); H_1—ditching depth (mm); x_1—ditching width (mm).

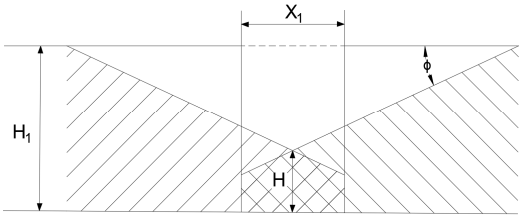


Figure 2. Self-covering depth of chisel-type furrow opener.

The width of the opener used in this study is 50 mm, and the penetration depth of the opener is 50 mm. By substituting Equation (1), the thickness of the self-covering soil of the opener is about 20 mm. It can be concluded that the self-covering effect of the opener is not significant enough to meet the requirements of seed thickness, so it is necessary to design the soil-covering device behind the opener.

The soil-dividing plate is installed on both sides of the rear end of the opener, and its basic function is to cover a small amount of small soil particles on the surface of the seeds to complete the first soil cover [26]. In order to enhance the diversion effect of the soil, the soil dividing plate is bent inward at an angle, and when the opener moves forward, the inner side pushes the finely divided soil on both sides of the seed ditch so that the soil slips relative to the soil dividing plate and falls into the ditch. Under the action of soil separation on the outer side of the soil separation plate, the soil block falls back to the seed furrow with a delay so that the finely divided soil is preferentially contacted with the seeds, and then the larger soil particles and soil blocks are covered on the top surface. In order to explore the structural design of the soil dividing plate, the force analysis of the soil dividing plate is carried out, refer to Figure 3.

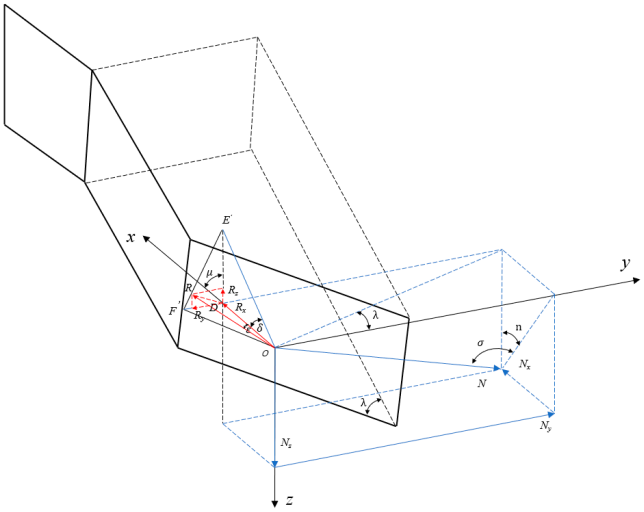


Figure 3. Force analysis diagram of dividing plate.

Select any point o of the soil-contacting part on the soil dividing plate as the research object, and establish a space rectangular coordinate system, as shown in Figure 3. The positive direction of the *x*-axis is the forward direction of the soil dividing plate, the normal stress of soil particles to the soil-dividing plate is σ, and the friction force is *R*. The triangle OE′F′ is the micro-element plane of the point O on the plane, and the friction force of the soil-dividing plate is analyzed based on the three-sided wedge OD′E′F′ [27]. On the triangle OE′F′, the friction force *R* is perpendicular to the straight line E′F′, and the angle ε between the friction force R and the *x*-direction is the minimum value. According to the resultant vector projection theorem, the relationship between the normal stress *N* and the friction force *R* projected in the x-direction is:

$$\begin{cases} \sigma_x = N \cos \mathrm{n} \sin \delta \\ R_x = R \cos \varepsilon \end{cases} \quad (2)$$

In the formula, σ_x is the component force of N in the x-direction, and the unit is *N*. R_x is the component force of the friction force *R* in the x-direction, and the unit is *N*. n is the angle between the normal stress N and the XOZ plane, the unit is (°). δ is the inclination angle of the soil dividing plate; the unit is (°).

From the geometric relationship, we can obtain:

$$\begin{cases} \tan\sigma = \frac{\sin\delta}{\tan\lambda} \\ \tan\varepsilon = \tan\delta\cos\mu \\ \tan\mu = \frac{\tan\delta}{\tan\lambda} \end{cases} \tag{3}$$

$$R_{fx} = \frac{N\tan\lambda\sin\delta}{\sqrt{\tan^2\lambda + \sin^2\delta}} + N\tan\varphi\sqrt{\frac{\tan^2\lambda\cos^2\delta + \sin^2\delta}{\tan^2\lambda + \sin^2\delta}} \tag{4}$$

It can be seen from Equation (4) that the normal stress N, the friction angle φ, the element line angle λ and the inclination angle δ jointly determine the size of the working resistance R_{fx} of the soil dividing plate.

The structural design of the soil dividing plate is shown in Figure 4. In the figure, $\angle\lambda$ is the inclination angle of the soil dividing plate, and $\angle\eta$ is the inner angle of the soil dividing plate. In order to ensure that the seeds fall in the seed furrow, the distance between the width of the opener and the inflection point of the soil-dividing plate must meet [26]:

$$60 \le H_1 + 2l_2 \le 80 \tag{5}$$

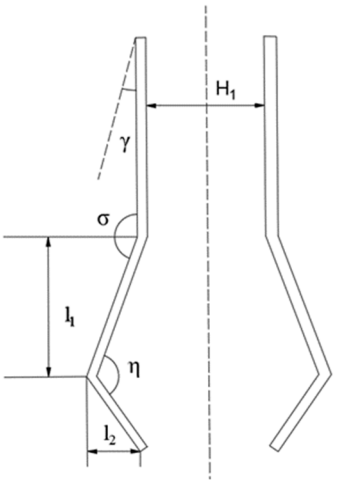


Figure 4. Structural design drawing of dividing plate.

The width H_1 of the opener designed in this paper is 40 mm. According to Equation (5), the value range of l_2 is 10–20 mm. In this paper, l_2 = 15 mm. According to the geometric relationship of the structure, the distance l_1 from the soil dividing plate to the inflection point is:

$$l_1 = \frac{l_2}{\tan(180^\circ - \sigma)} \tag{6}$$

According to Equation (6), l_1 is 44 mm. In order to ensure the smooth backfilling of the soil, the inclination angle λ of the soil dividing plate should be much larger than the friction angle between the soil and the shovel body.

The basic function of the soil-cover disc is to cover the soil on both sides of the opener to the top of the seeds and achieve a certain thickness of soil cover. In order to increase the amount of soil cover, two soil-cover discs were installed on the soil-cover frame to cover the seeds. The soil-covering discs also belong to the disc harrow category, and the relevant design parameters are calculated according to the empirical formula of concave disc design. The formula for calculating the diameter of the covering disc is as follows:

$$D = KB \tag{7}$$

In the formula: D is the diameter of the soil-covering disc, the unit is mm; K is the diameter-depth ratio coefficient; B is the designed soil depth, and the unit is mm. The designed soil-covering device is mainly aimed at the no-tillage sowing of corn. The sowing depth of corn is generally 30–50 mm, and the K value of the disc is generally 4–6 [24], so the diameter of the disc is designed to be 125 mm.

When the covering disk is cut into the soil, the force analysis is shown in Figure 5. During the soil-covering process, the soil-covering device moves forward with the speed V, P is the power of the tractor, and the pulling force is F_1. $\angle\alpha$ is the inclination angle of the soil-covering device, $\angle\beta$ is the opening angle of the soil-covering device, and the friction force F_f (excluding the force between the soils). The force F_A is:

$$F_A = F_N = \frac{P}{V} \tag{8}$$

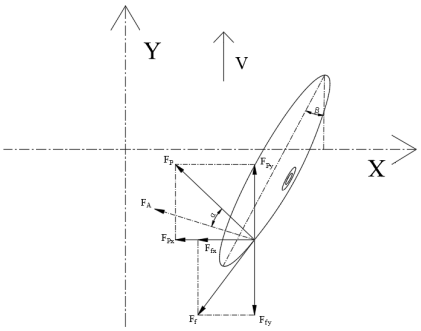


Figure 5. Force Analysis of Disc (the top view).

F_P is the component force of F_A on the plane XOY surface:

$$F_P = F_A \cos a \tag{9}$$

The friction force is:

$$F_f = \mu F_N \tag{10}$$

The force analysis of the covering disk along the y-axis direction is as follows:

$$F = F_1 + F_{py} - F_{fy} \tag{11}$$

In the formula: F is the resultant force on the covering disk in the y-axis direction; F_{py} is the y-axis component of the resultant pressure on the soil on the disk; F_{fy} is the y-axis component of the friction force between the soil and the disk.

Figure 6 is a schematic diagram of the grounding situation of the earth-covered disc, and the calculation formula of its grounding area is:

$$S = \frac{S_{ABC}}{\cos\beta} \tag{12}$$

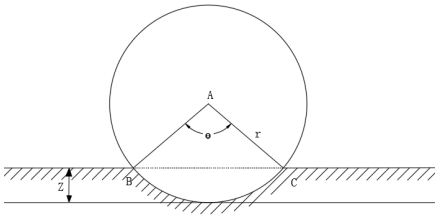


Figure 6. Schematic diagram of the effective area of the disc grounding.

The area of the arc in the formula is:

$$S_{ABC} = r^2 \cdot \left(\frac{\pi\theta}{360}\right) - \frac{1}{2} l_{AB}(r - z_0) \tag{13}$$

where:

$$l_{AB} = 2\mathrm{r}\sin\left(\frac{\theta}{2}\right) \tag{14}$$

$$\theta = 2\arccos\left(\frac{\mathrm{r} - Z_0}{\mathrm{r}}\right) \tag{15}$$

It can be seen from Equations (8) and (10) that the effect of soil covering is related to the structural parameters of the soil-covering device, soil conditions, and forward speed, and the specific influence law needs to be further studied through experiments.

2.2. Altair EDEM Simulation Analysis

2.2.1. Soil Particle Model

Relevant research shows that the no-till soil structure is mostly cemented into granules and small clumps; the soil is biased towards viscosity [28]. Combined computational efficiency and simulation effects. In this study, the soil particle model was set up as spherical particles with a particle size of 5 mm [29]. Particle-to-particle contact is selected to Hertz-Mindin with bonding contact model simulation [30,31]. All particles can be bonded together by setting up a bonding contact in the particle contact model to generate particle aggregates of other shapes.

2.2.2. Corn Grain Model

The brand of corn seeds used in this study was "Jade 188"; we randomly selected 100 corn seed pellets and measured their three-axis dimensions with a vernier caliper. The average of the measured corn seed height, width, and thickness was selected as the size of the corn pellet model. The length of the corn seeds was13 mm, the width was 9.5 mm, and the thickness was 4.5 mm.

A maize seed simulation model was established using the spherical particle polymer method [32–35]. First, we created a 3D model of corn seeds in Solid works. Then, we imported the corn seed 3D model into Altair EDEM, filled it with a large number of spherical particles and obtained a corn seed model. The corn grain model is shown in Figure 7.



(**a**) (**b**)

Figure 7. Corn grain model: (**a**) Actual corn seed; (**b**) Corn Seed Simulation Model.

2.2.3. Altair EDEM Simulation Parameters

Discrete element simulation parameters mainly include material parameters and contact mechanics parameters. Material parameters mainly include soil-covering device, soil, the density of corn seeds, Poisson's ratio, and shear modulus [36–38]. The contact mechanics parameters mainly include soil-to-soil, the recovery coefficient between the

covering device and the soil, the static friction coefficient, the rolling friction coefficient, etc. [39,40]. The remaining parameters are measured by rest angle, the inclined plate test and other physical and mechanical tests. The discrete element simulation time step was taken as 1×10^{-5} s, and the acceleration of gravity was 9.8 m·s^{-2}. The remaining main parameters are shown in Table 1.

Table 1. Basic Parameters of Discrete Element Models for Granular Materials and Covering Devices.

Parameter	Granular Material			Covering Device (Steel)	
	Soil		Corn		
density/(kg·m^{-3})	2600		1197	7800	
Poisson's ratio	0.5		0.4	0.3	
Modulus of shear/Pa	2×10^7		1.37×10^8	7.9×10^{10}	
	soil-soil	soil-corn	soil-steel	corn-corn	corn-steel
Recovery factor	0.2	0.068	0.1	0.182	0.456
coefficient of friction	0.25	0.698	0.2	0.2	0.436
Rolling coefficient of friction	0.04	0.155	0.02	0.0782	0.059

2.2.4. Altair EDEM Simulation

In order to meet the working conditions of simulation and reduce the experiment of simulation, the trough size (length × width × height) set in this study is 3000 mm × 1000 mm × 220 mm. Set the depth of the opener to 50mm. The total simulation time is 10 s, of which 0~5 s is the formation time of the bottom soil particles. During this period, 360,000 soil particles that meet the sowing conditions are generated, and the soil particles settle naturally for 1 s. The formation time of topsoil particles is 6~8 s; set the particle generation mode to random generation, and particle sizes are randomly generated in the range of 0.5 to 1.5 times the original particle radius. In order to make the small size particles fill the crevices of the large size soil particles as soon as possible and avoid forming too loose soil, the number of topsoil particles is set to 200,000. Soil particles settle naturally for 1 s. Apply Solid works 2021 software (Dassault Systemes, Vélizy-Villacoublay, France) to create geometric simulation models of coverers with different parameters. To facilitate the observation of the effect of the job and speed up the simulation time, compress the connecting parts of the cover when the simulation model is established, save the geometric simulation model in IGS format and import it into Altair EDEM.

A pellet generating module for corn seeds is set at the lower part of the seed meter, sets the total amount of grains generated for seeds to 150, and sets the pellet generation module forward speed of the corn seed to be the same as the forward speed of the cover device, maximum simulation of sowing and soil-covering process. At 9 s, the soil-covering device began to move, and the simulation ended at 12s. The simulated geometry of the trough and cover device is shown in Figure 8.

2.2.5. Particle Motion Mechanism Analysis

Soil particles located at the front of the opener during the soil-covering device with soil-closing function simulation are picked up by the tip of the shovel, and the soil particles picked up pass through the tip of the shovel. It moves along the retainer under the action of its weight, and surrounding soil, the diversion effect of the soil dividing plate is filled into the trench, after that, the soil is covered by the soil-covering discs, and the entire trenching and covering movement is completed. Figure 9a,c shows the vector distribution of soil particle velocity. Figure 9b,d shows the conventional double-disc covering device's soil particle velocity vector distribution. As seen from the comparison chart, soil-covering devices with soil-closing functions can enhance soil fluidity during no-till operations and cover the seed surface with fine soil fragments.

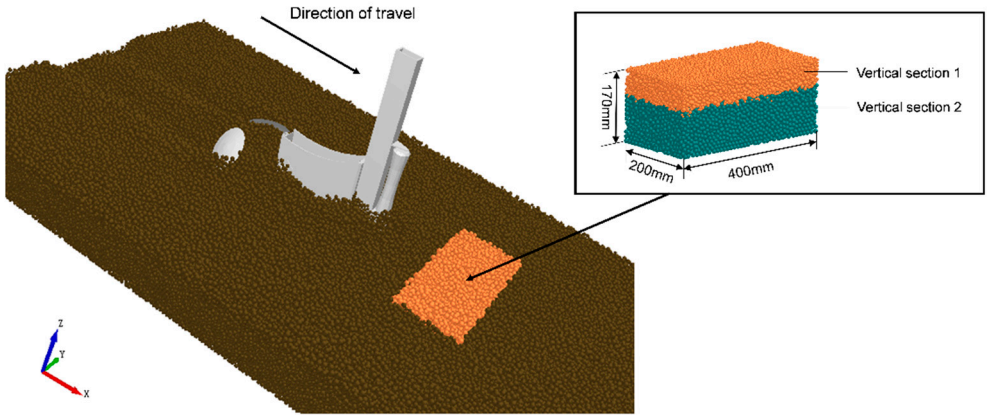


Figure 8. Simulation model of cover device and trough.

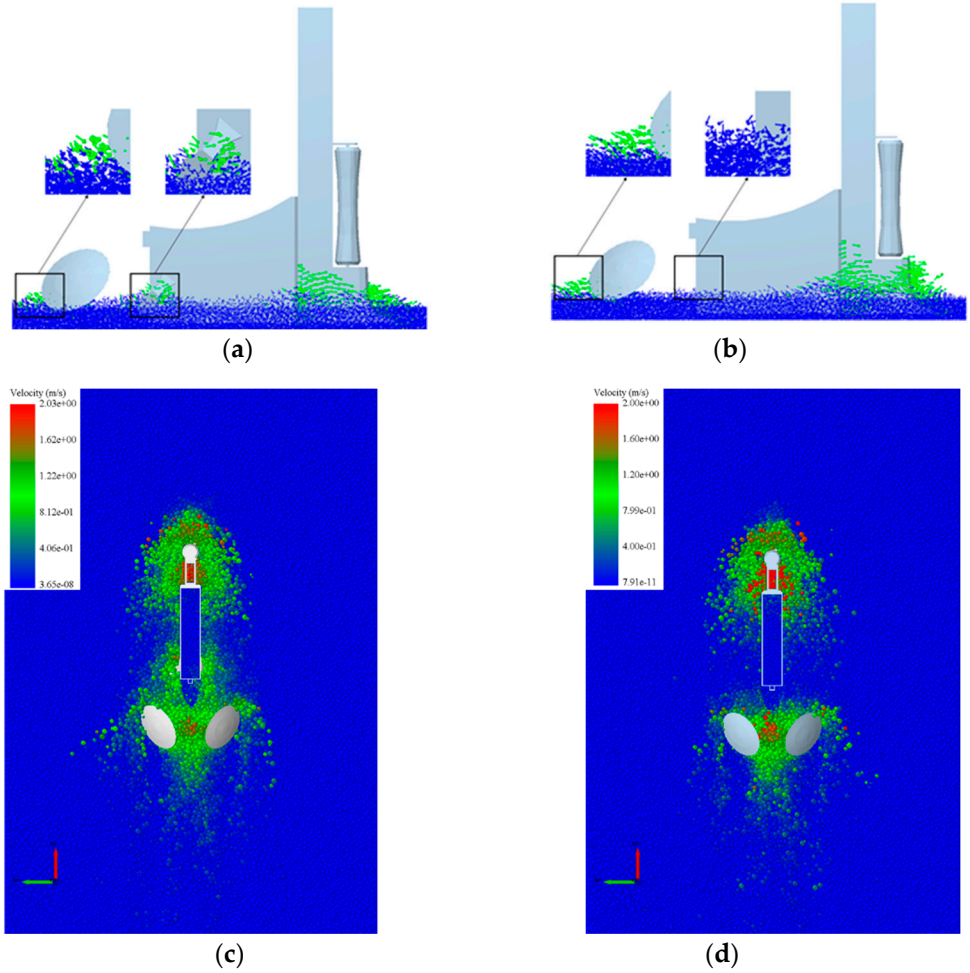


Figure 9. Comparison map of vector distribution of soil particle velocity: (**a**) Side view of the soil-covering device with soil-closing function from; (**b**) Side view of the Traditional double-disc soil-covering device; (**c**) Top view of the soil-covering device with soil-closing function from quarter view; (**d**) Top view of the traditional double disc soil-covering device.

As can be seen from the cover renderings of Figure 10, most of the smaller soil particles are located at the seed location when the soil is covered after the soil-covering process, while the larger soil particles cover the surface of the smaller soil particles. Therefore, it is shown that the soil-covering device with soil-closing function first uses the diversion effect of the soil-dividing plate to cover the soil once during the soil-covering process and then

uses the surface soil to complete the secondary cover is basically in line with the original design intention.

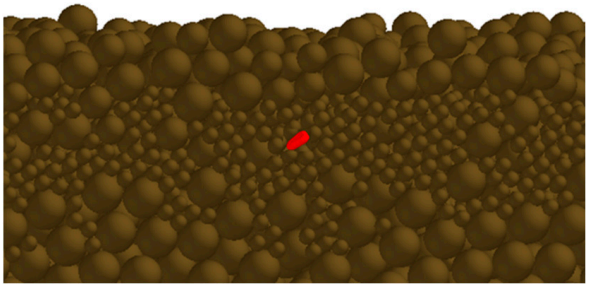


Figure 10. Effect drawing of covering soil. Red grains represent corn seed.

In order to explore the movement law of soil under the soil-covering device with a soil-closing function, it is necessary to ensure that the selected soil particles are approximately equal in the direction of the opener and the spacing of each soil particle. Five soil particles within the tillage depth range that meet the conditions were selected, and the selected soil particle distribution is shown in Figure 11. A soil particle is selected at each of the five locations for tracking its three-dimensional movement.

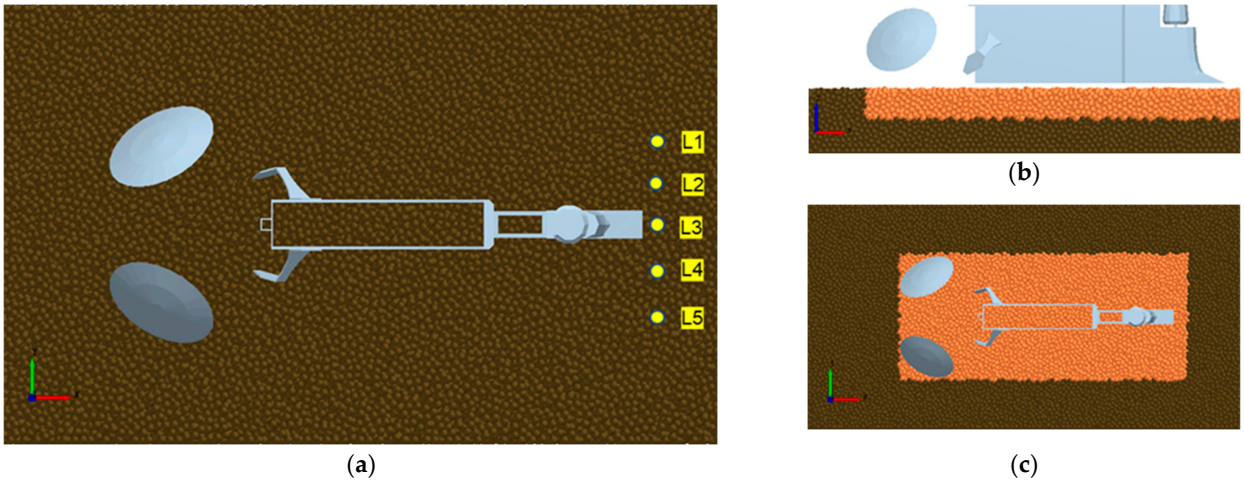


Figure 11. Particle distribution of soil: (**a**) Schematic diagram of soil particle distribution, L1–L5 were soil particles selected in sequence.; (**b**) Cross-sectional view of the soil covering a range of the soil-covering device; (**c**) Top view of the soil covering a range of the soil-covering device.

Solving the trench covering process, soil particles' horizontal, lateral and vertical motion displacement curves are obtained, as shown in Figure 12. By comparing the displacement curves of soil particles at the corresponding position in Figure 12, it is found that the soil particles move backward towards the bottom of the trench as the opener breaks the soil under the dynamic diversion of the soil coverer. As the tip of the shovel gradually approaches the selected soil particles, the soil particles collide under the action of the tip, and the soil particles begin to produce a motion trajectory in an obliquely upward direction. When the tip of the shovel passes through the soil particles, the particles move along the soil dividing plate, creating a diagonal downward movement into the seed ditch. After the soil particles enter the seed ditch, they are gently covered and stop moving under the action of the soil-covering disk, completing the entire soil-covering process.

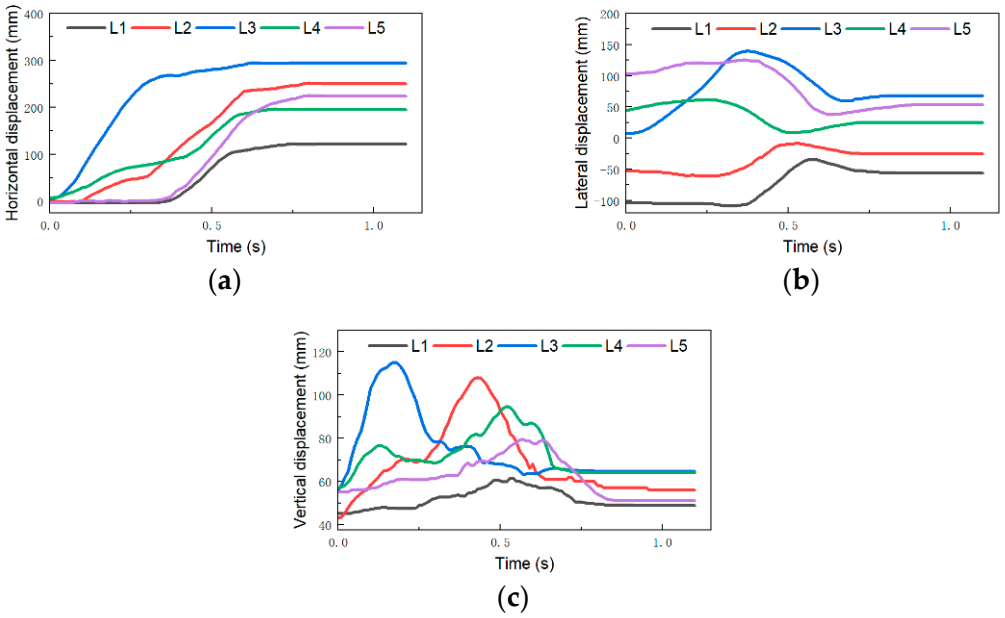


Figure 12. The motion curves of soil particles at different locations during tillage: (**a**) movement curve of soil particles along the x-direction; (**b**) movement curve of soil particles along the y-direction; (**c**) Movement curve of soil particles along the x-direction.

3. Results

3.1. Simulation Test of Soil-Covering Device

The soil-covering device is one of the important working parts of the precision seeding machine. It is used to cover the seeds in the seed trench and achieve the purpose of suitable thickness and uniform soil cover. The performance of the soil-covering device mainly depends on its structural parameters and motion parameters, reducing the positional deviation of the seeds moving with the soil flow, and improving the precision seeding theory. Therefore, in this study, the thickness of the seed covering soil H and the seed offset X were selected as the evaluation indicators of the performance of the covering soil device.

Seed cover thickness refers to the thickness of the soil cover above the seeds. After ditching, select the center of the seed as the measurement reference point, measure the thickness H of the soil covered above the seed, measure five times, and take the average of the results. The soil section after the simulation operation is analyzed through the clipping module in the Altair EDEM post-processing, and the thickness H of the seed covering soil is measured with the scale that comes with the software.

Seed offset refers to the positional deviation of seeds following soil flow after they touch the soil. The *x*-axis and *y*-axis coordinates of the corn seeds are exported in the Altair EDEM post-processing interface, and the seed offset x is calculated according to the *y*-axis coordinates of the corn seeds.

3.2. Quadratic Orthogonal Rotational Regression Combined Experimental Design

In order to further study the influence of the soil shunt cover's structural parameters on the seed cover's thickness and the seed's displacement, the quadratic orthogonal rotation regression combination test was carried out using the Altair EDEM 2020 simulation software (DEM Solutions, Edinbrugh, UK). Four key parameters (X1, X2, X3, X4) that affect the soil-covering effect are selected as factors. The thickness of seed covering soil and seed displacement were selected as the test indicators. The quadratic orthogonal rotation regression combination test with four factors and three levels was designed by Design-expert 10 software (Stat-Ease; Minneapolis, MN, USA) to study the relationship between the key factors and the test indicators. Set the depth into the soil to 50mm, select the

diameter D of the disc to be 125mm, and the opener width to 50mm. The orthogonal test factors and levels are shown in Table 2 [41,42].

Table 2. Factors and Levels of Quadratic Orthogonal Rotational Regression Combination Test of Operation Effect of Soil-Covering Device.

Factor Level	Working Speed ($km \cdot h^{-1}$)	The Opening Angle of the Disc (°)	The Inclination Angle of the Disc (°)	The Inclination Angle of the Soil Dividing Plate (°)
−1	3	60	65	40
0	5	65	70	45
1	7	70	75	50

3.3. Simulation Test Results and Analysis

The test results are shown in Table 3. Among them, X1, X2, X3, and X4 are the coding values of operating speed, disc opening angle, disc inclination angle, and soil-dividing plate inclination angle, respectively.

Table 3. Scheme and Results of Quadratic Orthogonal Rotation Regression Combination Test of Soil-covering Device Operation Effect.

Test Serial Number	Factor				Soil-Covering Thickness /Y_1(mm)	Seed Offset /Y_2(mm)
	Working Speed /x_1($km \cdot h^{-1}$)	The Opening Angle of the Disc /x_2(°)	The Inclination Angle of the Disc /x_3(°)	The Inclination Angle of the Dividing Plate /x_4(°)		
1	7	70	70	45	47.5	31.2
2	3	65	70	40	41.2	24.3
3	5	65	70	45	52.4	25.4
4	7	60	70	45	52.1	21.6
5	5	65	65	40	51.5	18.5
6	7	65	70	50	44.3	39.5
7	3	60	70	45	36.8	13.8
8	3	65	65	45	45.2	14.2
9	7	65	70	40	45.3	14.7
10	5	65	70	45	52.2	25.0
11	5	65	75	50	40.8	32.0
12	3	65	75	45	31.4	13.3
13	7	65	75	45	42.8	35.9
14	7	65	65	45	48.2	37.5
15	5	65	65	50	52.6	35.0
16	5	60	70	40	46.8	18.2
17	3	65	70	50	36.5	10.2
18	5	70	70	50	51.0	21.4
19	5	65	70	45	48.2	18.1
20	5	70	70	40	52.3	25.6
21	5	70	75	45	44.3	28.6
22	5	60	65	45	41.9	21.9
23	5	65	70	45	51.2	16.6
24	5	60	70	50	46.6	20.2
25	5	70	65	45	49.5	31.4
26	5	60	75	45	40.8	19.7
27	5	65	70	45	50.5	18.3
28	5	65	75	40	42.8	15.6
29	3	70	70	45	45.0	17.7

3.3.1. Regression Equation

Design-Expert10 software was used to analyze the experimental data, and the F test was performed under the confidence level $\alpha = 0.05$. The partial sum of squares and degrees of freedom of insignificant factors and interactions were incorporated into the remaining sum of squares, and the analysis was performed again [42]. Ensure that all factors reach a significant or extremely significant level and obtain the optimized regression equation:

$$Y_1 = 50.90 + 3.66x_1 + 2.05x_2 - 3.83x_3 - 0.68x_4 - 3.20x_1x_2 + 2.10X_1X_3 + 0.93x_1x_4 - 1.03x_2x_3 - 0.28x_2x_4 - 0.78x_3x_4 - 5.80x_1^2 - 1.01x_2^2 - 3.86x_3^2 - 1.38x_4^2 \quad (16)$$

$$Y_2 = 2.07 + 0.72x_1 + 0.34x_2 - 0.11x_3 + 0.35x_4 + 0.14x_1x_2 - 0.018x_1x_3 + 0.97x_1x_4 - 0.015x_2x_3 - 0.15x_2x_4 - 0.0025x_3x_4 + 0.048{x_1}^2 + 0.016{x_2}^2 + 0.42{x_3}^2 + 0.064{x_4}^2 \quad (17)$$

3.3.2. Analysis of Variance of the Regression Equation

It can be seen from Tables 4 and 5 that the regression models of the two indicators are extremely significant ($p < 0.01$), indicating that the selected model is appropriate, and there is a model-determined relationship between the test indicators and the test factors. At the same time, the lack of fit terms was not significant ($p > 0.1$), indicating that the model was suitable, no uncontrolled factors influenced the indicators, and the fitting effect of the model was good. From the regression model in Table 4, it can be seen that the proportion of the influence of the thickness of the covering soil is the inclination angle of the disc, the working speed, the opening angle of the disc, and the inclination angle of the soil dividing plate. The regression model in Table 5 shows that the proportion of the influence of seed offset is the operating speed, the inclination angle of the soil dividing plate, the disc opening angle and the disc inclination angle.

Table 4. Analysis of variance for regression model of covering soil thickness.

Project	Squares	df	Square	F	P
Model	734.42	14	52.46	7.11	0.0004
x_1	162.07	1	162.07	21.95	0.0004
x_2	50.46	1	50.43	6.83	0.0204
x_3	176.33	1	176.33	23.89	0.0002
x_4	5.47	1	5.47	0.74	0.4040
x_1x_2	40.96	1	40.96	5.55	0.0336
x_1x_3	17.64	1	17.64	2.39	0.1445
x_1x_4	3.42	1	3.42	0.46	0.5070
x_2x_3	4.20	1	4.20	0.57	0.4631
x_2x_4	0.30	1	0.30	0.041	0.8425
x_3x_4	2.40	1	2.40	0.33	0.5774
${x_1}^2$	217.89	1	217.89	29.52	<0.0001
${x_2}^2$	6.60	1	6.60	0.89	0.3606
${x_3}^2$	96.56	1	96.56	13.08	0.0028
${x_4}^2$	12.19	1	12.19	1.65	002197
Residual	103.35	14	7.38		
Lack of Fit	91.87	10	9.19	3.20	0.1367
Pure Error	11.48	4	2.87		
Cor Total	837.77	28			

Table 5. Regression model analysis of Variance for Seed Offset.

Project	Squares	df	Square	F	P
Model	14.37	14	1.03	4.10	0.0063
x_1	6.29	1	6.29	25.13	0.0002
x_2	1.37	1	1.37	5.46	0.0349
x_3	0.15	1	0.15	0.60	0.4524
x_4	1.43	1	1.43	5.70	0.0316
x_1x_2	0.081	1	0.08	0.324	0.5780
x_1x_3	0.0012	1	0.0012	0.0049	0.9452
x_1x_4	3.78	1	3.78	15.10	0.0016
x_2x_3	0.001	1	0.0009	0.0035	0.9530
x_2x_4	0.0961	1	0.0961	0.384	0.5456
x_3x_4	2.5×10^{-5}	1	2.5×10^{-5}	9.98×10^{-5}	0.9922
x_1^2	0.015	1	0.015	0.060	0.8102
x_2^2	0.0016	1	0.0016	0.0063	0.9379
x_3^2	1.14	1	1.14	4.55	0.0510
x_4^2	0.027	1	0.0268	0.107	0.7482
Residual	3.51	14	0.25		
Lack of Fit	2.81	10	0.28	1.61	0.3431
Pure Error	0.70	4	0.17		
Cor Total	17.88	28			

3.3.3. Response Surface Analysis of Each Test Factor to Test Index

The influence rule of factor interaction and test index is shown in Figure 13. It can be seen from Figure 13a that when the opening angle of the disc is constant, the thickness of the covering soil increases sharply at first and then tends to be gentle; when the working speed is constant, the thickness of the covering soil increases with the increase in the opening angle of the disc. It can be seen from Figure 13b that when the working speed is constant, the thickness of the covering soil changes little with the increase of the inclination angle of the soil dividing plate; when the inclination angle of the soil dividing plate is constant, the thickness of the covering soil increases with the increase of the working speed. It can be seen from Figure 13c that when the inclination angle of the disc is constant, the relationship between the seed offset and the working speed tends to be linear and, at the same time, increases with the increase in the inclination angle of the disc; when the working speed is constant, the seed offset first decreases with the inclination angle of the disc increase after. It can be seen from Figure 13d that when the inclination angle of the disc is constant, the relationship between the seed displacement and the inclination angle of the soil dividing plate tends to be linear and increases with the increase in the inclination angle of the soil dividing plate; when the inclination angle of the soil dividing plate is constant, the seed displacement increases with the changing trend of the inclination angle of the disk is small, and it first decreases and then increases with the increase in the inclination angle of the disk.

3.3.4. Optimization of Structural Parameters

Through the optimization module in Design-expert, the optimal design is carried out with the covering soil thickness of 50 mm and the seed offset as small as possible. The optimal parameter combination is as follows; the operating speed was 6.35 km·h. The opening angle was 60°, the inclination angle of the disc was 70°, and the inclination angle of the soil plate is 40°; at this time, the thickness of the covering soil was 48.24 mm, and the seed offset was 10.67 mm, which meets the agronomic requirements of precision seeding operations [43].

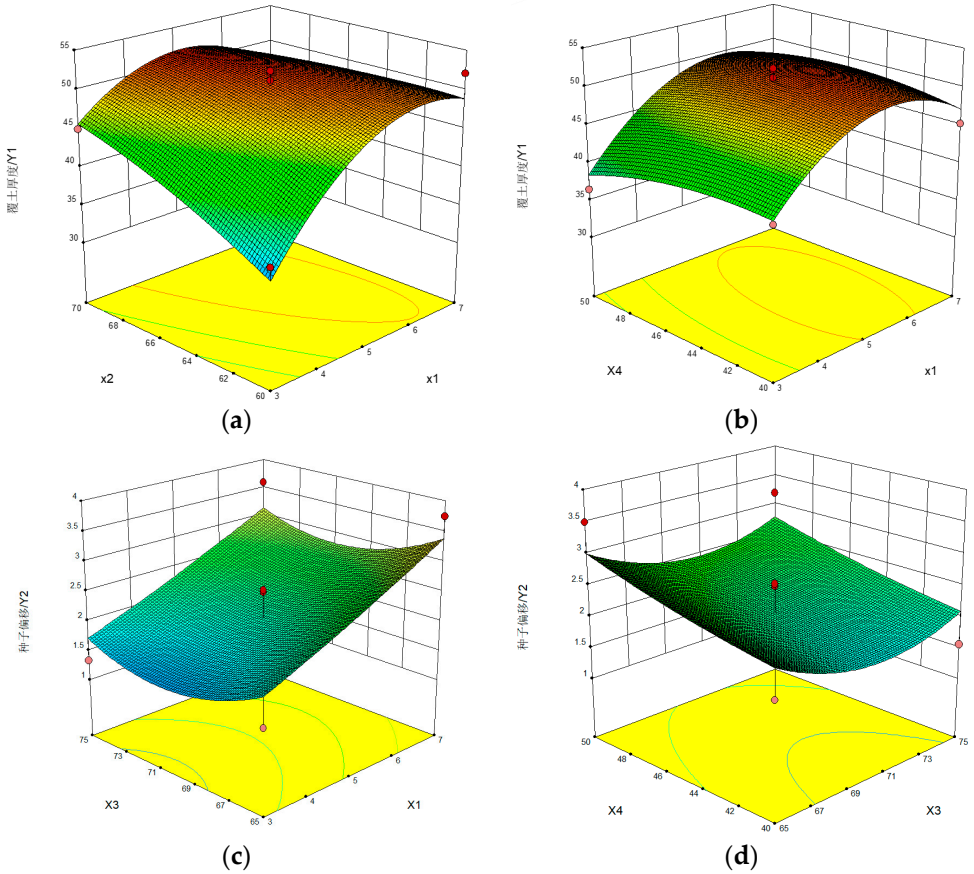


Figure 13. The interaction between the factors affects the response surface of the test index: (**a**) x3 and x4 are 70° and 45°, respectively, the relationship between the thickness of the covering soil and X1 X2; (**b**) X2 and X3 are 65° and 70°, respectively, the relationship between the thickness of the covering soil and X1 X4; (**c**) 2 and X4 are 65° and 45°, respectively, the relationship between the seed offset and X1 X3; (**d**) X1 and X2 are 3 km·h^{-2} and 65°, respectively, the relationship between the seed offset and X3 X4.

3.4. Field Test of the Soil-Covering Device

In order to test the working performance of the soil-covering device, the working performance test was carried out in the soil tank test base of the School of Agricultural Engineering and Food Science, Shandong University of Technology (Zibo, China). In order to test the performance of the soil shunt cover device compared with the traditional soil cover device, a comparative test was carried out. The biggest difference between the device we designed and optimized and the traditional soil-covering device is the presence or absence of the soil-dividing plate. Therefore, we conducted experiments by adding and removing the soil dividing plate.

3.4.1. Comparative Test

The performance test was carried out in the Agricultural Machinery Equipment Laboratory of Shandong University of Technology, as shown in Figure 14. Test conditions: the length × width of the soil tank was 8 × 1.5 m, the soil bulk density of 0–10 cm was 1522 Kg·m^{-3}, and the average moisture content was 15%. Test equipment included a soil tank test bench, corn no-tillage seeding monomer, TZS-IIWX soil moisture and temperature measuring instrument, TYD-2 soil compaction instrument, and ruler.

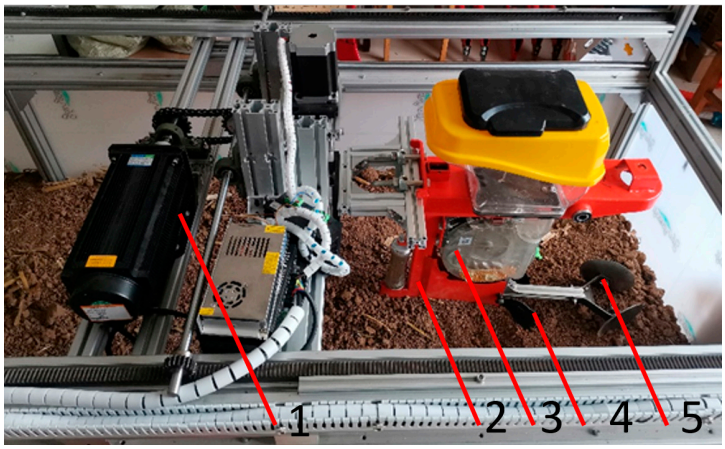


Figure 14. Equipment for soil tank test: 1—motor; 2—opener; 3—seed metering device; 4—dividing plate; 5—covering disc.

After installing the designed soil shunt type soil cover and the traditional disc type soil cover device, respectively, on the corn no-tillage seeding unit to carry out the field test operation, the section of the soil groove was manually intercepted. On the section made, we used a brush to gently find the seeds on the section and used a ruler to measure the distance H from the seeds to the soil surface, where H was the soil cover thickness. At the same time, we marked the landing position of the seeds during seeding. After the soil covering was completed, we used a ruler to measure the distance between the marked point and the actual position of the seeds to obtain the offset of the seeds and measured five times at different position.

It can be seen from Tables 6 and 7 that the difference in the soil-covering thickness of the soil shunt type covering device was 48.3–52.4 mm, that of the traditional covering device was 38.6–56.4 mm, and that of the combined soil-covering device was 12~20 mm, and the difference of seed offset of traditional soil-covering device was 25~53 mm. The test results show that the soil-covering device with a soil-closing function is better than the traditional soil-cover device. At the same time, the soil-covering device with a soil-closing function has the function of returning finely crushed soil, and the rationality of the design is also verified. The test results provide a guarantee for future tests.

Table 6. The measurement results of the difference in the thickness of the covering soil at the sampling point.

Types of Soil-Covering Device	Unit	Test Serial Number	Sampling Point				
			1	2	3	4	5
soil-covering device with soil-closing function	mm	1	53.1	52.6	50.6	62.2	55.2
		2	48.3	39.3	42.5	46.7	52.4
		3	52.2	53.0	49.7	48.3	38.2
		average value	51.2	48.3	47.6	52.4	48.6
Traditional double-disc soil-covering device	mm	1	43.6	50.4	59.3	65.8	41.2
		2	40.5	38.6	58.5	62.8	51.2
		3	31.7	37.9	48.7	40.6	45.0
		average value	38.6	42.3	55.5	56.4	45.8

Table 7. Measurement results of seed offset difference at the sampling point.

Types of Soil-Covering Device	Unit	Test Serial Number	Sampling Point				
			1	2	3	4	5
soil-covering device with soil-closing function	mm	1	22	24	24	15	12
		2	14	18	16	7	12
		3	12	18	14	14	21
		average value	16	20	18	12	15
Traditional double-disc soil-covering device	mm	1	30	63	31	54	48
		2	32	15	54	39	57
		3	13	36	23	66	33
		average value	25	38	36	53	46

3.4.2. Performance Test

The field experiment was carried out according to the optimal parameter combination obtained by the simulation experiment, the verification experiment was repeated three times, and five test points were taken each time. The experimental verification results and simulation optimization results are shown in Figure 15.

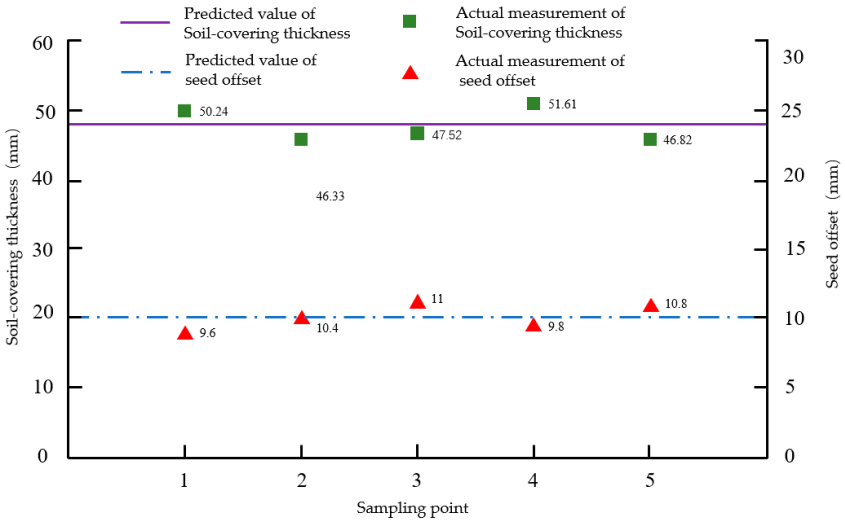


Figure 15. Test verification diagram.

It can be seen from Figure 15 that the difference between the simulation results and the results measured in the field test is small, the maximum relative error of the covering soil thickness is 5.7%, and the maximum error of the seed offset is 11.1%, which shows the reliability of the experimental optimization results, and also verifies the feasibility of the simulation.

4. Discussion

The changing trend of the response surface analysis shown in Figure 11 indicates that the higher the working speed, the better the soil-breaking performance of the opener, and the greater the soil disturbance. However, an excessively high working speed will bring about excessive power consumption; thus, it is generally advisable to use a working speed that can ensure the covering soil thickness Y1 = 50 mm, 10% floating up and down. Moreover, the working speed is too high, the soil cannot be completely covered in a short time, resulting in poor soil-covering effect, thus reducing the covering soil thickness Y1, so the working speed of the planter should not be too high.

Considering the changes in the trend of the evaluation index Y2 in Figure 11, we concluded that with the increase in working speed, the fluidity of soil increases, which

leads to the increase in seed offset Y2, which causes the uniformity of seed arrangement to decrease. In addition, the smaller the inclination angle x4 of the soil dividing plate is, the more stable the soil fluidity of the seed furrow will be, resulting in the smaller seed offset Y2; but if the inclination angle x4 of the soil dividing plate is too small, the amount of flowing soil at the soil dividing plate will increase, and the soil dividing plate cannot withstand a large amount of soil in a short time. This will easily cause the soil to block at the soil dividing board, resulting in a decrease in the thickness of the covering soil Y1, and the thickness of the covering soil cannot be guaranteed.

Further in-depth analysis showed that the change rate of the response surface of the evaluation indicator Y2 in the direction of the working speed and the inclination angle of the soil-dividing plate is better than the change rate of the response surface in the direction of the opening angle of the disc and the inclination angle of the disc. It shows that in this interaction, the influence of the working speed x1 and the inclination angle of the soil-dividing plate x4 on the seed offset Y2 is more significant. x1 and x4 were the dominant factors affecting the inter-row straw mulching Y2.

5. Conclusions

(1) A soil-covering device with a soil-closing function that can realize the separation of clod and fine soil and the angle of soil covering can be adjusted is designed, the key parameters of the device were designed, and the interaction model between the soil-covering device and the soil was established.

(2) The quadratic rotation regression combination orthogonal was used to conduct the simulation test. The primary and secondary order of the factors affecting the performance of the soil-covering device was obtained through variance analysis and response surface analysis: speed, disc opening angle, soil dividing plate inclination angle, and disc inclination angle. The optimal combination was as follows: the operating speed was 6.35 $km \cdot h^{-1}$, the disc opening angle was 60°, the disc inclination angle was 70°, and the soil plate inclination angle was 40°. Currently, the covering soil thickness was 48.24 mm, and the seed offset is10.667 mm.

(3) Through comparative experiments, it was determined that the soil-covering device with a soil-closing function could separate soil blocks and enhance the performance of soil fluidity. The results show that the thickness of soil cover was 48.3–52.4 mm, and the seed offset was 12–20 mm. The seed offset was small, and the soil covering was uniform, which meets the agronomic requirements of corn planting.

Author Contributions: Conceptualization, Y.G. and X.W.; methodology, X.W.; software, Y.G. and X.Z. (Xiaokang Zhong); experiment, K.C. and Y.G.; data curation, Y.G. and X.Z. (Xiaokang Zhong); writing—original draft preparation, Y.G. and X.Z. (Xiaokang Zhong); writing—review and editing, K.C. and Q.L.; visualization, X.Z. (Xiangcai Zhang); supervision, Z.W.; project administration, X.W.; funding acquisition, M.W. and X.C. All authors have read and agreed to the published version of the manuscript.

Funding: This work was supported financially by the National Natural Science Foundation of China (Grant No. 32101631).

Institutional Review Board Statement: Not applicable.

Informed Consent Statement: Not applicable.

Data Availability Statement: Not applicable.

Acknowledgments: The authors would like to thank the teachers and supervisors for their technical support. We would also like to acknowledge the assistance provided by brothers and sisters during the tests. Finally, we are grateful to the editor and anonymous reviewers for providing helpful suggestions to improve the quality of this paper.

Conflicts of Interest: The authors declare no conflict of interest.

References

1. Wang, Q.; Cao, X.; Wang, C.; Li, H.; He, J.; Lu, C. Research Progress of No/Minimum Tillage Corn Seeding Technology and Machine in Northeast Black Land of China. *Trans. Chin. Soc. Agric. Mach.* **2021**, *52*, 1–15.
2. Wang, Q.; Xu, Q.; Lu, C.; Li, H.; He, J.; Wang, Q. Research status and development of key technologies for no-tillage seeding intellectualization. *J. South China Agric. Univ.* **2021**, *42*, 27–35.
3. Somerville, P.D.; May, P.B.; Livesley, S.J. Effects of deep tillage and municipal green waste compost amendments on soil properties and tree growth in compacted urban soils. *J. Environ. Manag.* **2018**, *227*, 365–374. [CrossRef] [PubMed]
4. Hargreaves, P.R.; Baker, K.L.; Graceson, A.; Bonnett, S.; Ball, B.C.; Cloy, J.M. Soil compaction effects on grassland silage yields and soil structure under different levels of compaction over three years. *Eur. J. Agron.* **2019**, *109*, 125916. [CrossRef]
5. Liu, L.; Ma, C.; Liu, Z. EDEM-based Parameter Optimization and Experiment of Full-layer Fertilization Shovel for Strip Subsoiling. *Trans. Chin. Soc. Agric. Mach.* **2021**, *10*, 74–83.
6. Yan, B.; Wu, G.; Fu, W.; Gao, N.; Meng, Z.; Zhu, P. Influencing Factors of Corn Implantation Distribution for High-Planting Based on EDEM. *Trans. Chin. Soc. Agric. Mach.* **2020**, *51*, 47–54.
7. Chen, Y.; Munkholm, L.J.; Nyord, T. A discrete element model for soil–sweep interaction in three different soils. *Soil Tillage Res.* **2013**, *126*, 34–41. [CrossRef]
8. Ucgul, M.; Saunders, C. Simulation of tillage forces and furrow profile during soil-mouldboard plough interaction using discrete element modelling. *Biosyst. Eng.* **2020**, *190*, 58–70. [CrossRef]
9. Tekeste, M.Z.; Balvanz, L.R.; Hatfield, J.L.; Ghorbani, S. Discrete element modeling of cultivator sweep-to-soil interaction: Worn and hardened edges effects on soil-tool forces and soil flow. *J. Terramechanics* **2019**, *82*, 1–11. [CrossRef]
10. Hang, C.; Gao, X.; Yuan, M.; Huang, Y.; Zhu, R. Discrete element simulations and experiments of soil disturbance as affected by the tine spacing of subsoiler. *Biosyst. Eng.* **2018**, *168*, 73–82. [CrossRef]
11. Barr, J.; Desbiolles, J.; Ucgul, M.; Fielke, J.M. Bentleg furrow opener performance analysis using the discrete element method. *Biosyst. Eng.* **2020**, *189*, 99–115. [CrossRef]
12. Zhang, H.; Chen, J.; Song, Y.; Han, D.; Ji, C. Design of Auger Screw Precise Soil Covering Device for Dry Land. *Xinjiang Agric. Mech.* **2021**, *5*, 21–22.
13. Zhang, Z.; Sun, X.; Jin, Z.; Bing, Z.; Sun, J.; Tong, J. Design and Test of Crushing Bionic Soil Covering Device of Soybean Seeder. *Trans. Chin. Soc. Agric. Mach.* **2018**, *49*, 34–40, 73.
14. Lin, J.; Meng, F.; Gao, W. Optimum Design and Experimental Study of Soil Covering Device of Straw Deep-buried Returning Machine. *J. Shenyang Agric. Univ.* **2019**, *50*, 694–702.
15. Liu, X.; Jin, L.; Zhao, Y.; Guo, H.; Wang, J. Experiment research of double-deck disk coverer based on uniform design. *J. Chin. Agric. Mech.* **2016**, *37*, 26–28.
16. Song, L.; Yang, X.; Li, Q. Simulation study on precision seeding disc covering device based on SPH's mesh less method. *J. Chin. Agric. Mech.* **2016**, *37*, 29–32, 42.
17. Gou, W.; Ma, R.; Fan, G.; Yang, W.; Liu, L.; Lei, X. Parameter optimization of interlink covering device in relay-cropping system. *Trans. CSAE* **2011**, *27*, 33–37.
18. Wang, J. *The Research of Position Control after Seed Contacting Soil in the Process of Soil Covering and Rolling with Precision Seeder*; Jilin University: Jilin, China, 2012.
19. Li, Y.; Meng, P.; Geng, D.; He, K.; Meng, F.; Jiang, M. Intelligent System for Adjusting and Controlling Corn Seeding Depth. *Trans. Chin. Soc. Agric. Mach.* **2016**, *47*, 62–68.
20. Chao, B.; Yuang, P.; Han, C.; You, J.; Gao, J. Design of Automatic Regulating Device for Soil Cover of Transplanter. *J. Agric. Mech. Res.* **2022**, *44*, 54–58.
21. Nielsen, S.K.; Nørremark, M.; Green, O. Sensor and control for consistent seed drill coulter depth. *Comput. Electron. Agric.* **2016**, *127*, 690–698. [CrossRef]
22. Suomi, P.; Oksanen, T. Automatic working depth control for seed drill using ISO 11783 remote control messages. *Comput. Electron. Agric.* **2015**, *116*, 30–35. [CrossRef]
23. Kiani, S.; Kamgar, S.; Raoufat, M. Automatic on-line depth control of seeding unit using a non-contacting ultrasonic sensor. *Can. Soc. Bioeng.* **2010**, *6*, 13–17.
24. Kirkegaard Nielsen, S.; Munkholm, L.J.; Lamandé, M.; Nørremark, M.; Skou-Nielsen, N.; Edwards, G.T.C.; Green, O. Seed drill instrumentation for spatial coulter depth measurements. *Comput. Electron. Agric.* **2017**, *141*, 207–214. [CrossRef]
25. Chinese Academy of Agricultural Mechanization Sciences. *Agricultural Machinery Design Manual*; Chinese Agricultural Sientech Press: Beijing, China, 2007; pp. 343–389.
26. Liu, X.; Wang, X.; Chen, L.; Zhang, C.; Liu, W.; Ding, Y. Design and experiments of layered and quantitative fertilization device for rapeseed seeder. *Trans. CSAE* **2021**, *37*, 1–10.
27. Zhao, S.; Liu, H.; Yang, C.; Yang, L.; Gao, L.; Yang, Y. Design and Discrete Element Simulation of Interactive Layered Subsoiler with Maize Straw Returned to Filed. *Trans. Chin. Soc. Agric. Mach.* **2021**, *52*, 75–87.
28. Wang, Y. *Simulation Analysis of Structure and Effect of the Subsoiler Based on DEM*; Jilin Agricultural University: Jilin, China, 2014.
29. Ma, Y.; Wang, A.; Zhao, J.; Hao, J.; Li, J.; Ma, L.; Zhao, W.; Wu, Y. Simulation analysis and experiment of drag reduction effect of convex blade subsoiler based on discrete element method. *Trans. CSAE* **2019**, *35*, 16–23.
30. Potyondy, D.O.; Cundall, P.A. A bonded-particle model for rock. *Int. J. Rock Mech. Min. Sci.* **2004**, *41*, 1329–1364. [CrossRef]

31. Zhao, S.; Liu, H.; Tan, H.; Cao, X.; Zhang, X.; Yang, Y. Design and performance experiment of opener based on bionic sailfish head curve. *Trans. CSAE* **2017**, *33*, 32–39.
32. Shi, L.; Wu, J.; Sun, W.; Zhang, F.; Sun, B.; Liu, Q.; Zhao, W. Simulation test for metering process of horizontal disc precision metering device based on discrete element method. *Trans. CSAE* **2014**, *30*, 40–48.
33. Markauskas, D.; Ramírez-Gómez, Á.; Kačianauskas, R.; Zdancevičius, E. Maize grain shape approaches for DEM modelling. *Comput. Electron. Agric.* **2015**, *118*, 247–258. [CrossRef]
34. Barrios, G.K.P.; de Carvalho, R.M.; Kwade, A.; Tavares, L.M. Contact parameter estimation for DEM simulation of iron ore pellet handling. *Powder Technol.* **2013**, *248*, 84–93. [CrossRef]
35. Masson, S.; Martinez, J. Effect of particle mechanical properties on silo flow and stresses from distinct element simulations. *Powder Technol.* **2000**, *109*, 164–178. [CrossRef]
36. Wang, Y.; Liang, Z.; Zhang, D.; Cui, T.; Shi, S.; Li, K.; Yang, L. Calibration method of contact characteristic parameters for corn seeds based on EDEM. *Trans. CSAE* **2016**, *32*, 36–42.
37. Cui, T.; Liu, J.; Yang, L.; Zhang, D.; Zhang, R.; Lan, W. Experiment and simulation of rolling friction characteristic of corn seed based on high-speed photography. *Trans. CSAE* **2013**, *29*, 34–41.
38. Wang, J.; Tang, H.; Wang, Q.; Zhou, W.; Yang, W.; Shen, H. Numerical simulation and experiment on seeding performance of pickup finger precision seed-metering device based on EDEM. *Trans. CSAE* **2015**, *31*, 43–50.
39. Wang, X.; Zhong, X.; Geng, Y.; Wei, Z.; Hu, H.; Geng, D.; Zhang, X. Construction and parameter calibration of the nonlinear elastoplastic discrete element model for no-tillage soil compaction. *Trans. CSAE* **2021**, *37*, 100–107.
40. Huang, Y.; Hang, C.; Yuan, M.; Wang, B.; Zhu, R. Discrete Element Simulation and Experiment on Disturbance Behavior of Subsoiling. *Trans. Chin. Soc. Agric. Mach.* **2016**, *47*, 80–88.
41. Shi, Y.; Yu, H.; Jiang, Y.; Wang, X.; Chen, H.; Liu, H. Optimization of Strip Fertilization Planter for Straw Throwing and Paving. *Agriculture* **2022**, *12*, 613. [CrossRef]
42. Liu, H.; Hang, J.; Chen, J.; Lu, J.; Zhao, S. Performance Simulation and Experiment on Rigid Press Wheel for Hilly Area. *Trans. Chin. Soc. Agric. Mach.* **2018**, *49*, 114–122.
43. Zhou, L. *DEM-Based Modelling of Maize Seeds and the Simulation Analysis and Experimental Study of the Seed-Sowing*; Jilin Agricultural University: Jilin, China, 2021.